A relaxation-assisted 2D IR spectroscopy method

Dmitry V. Kurochkin, Sri Ram G. Naraharisetty, and Igor V. Rubtsov[†]

Department of Chemistry, Tulane University, New Orleans, LA 70118

A method of two-dimensional infrared (2D IR) spectroscopy called relaxation-assisted 2D IR (RA 2DIR) is proposed that utilizes vibrational energy relaxation transport in molecules to enhance cross-peak amplitudes. This method substantially increases the range of distances accessible by 2D IR and is capable of identifying long-range connectivity patterns in molecules. RA 2DIR is illustrated in interactions among CN and CO modes in 3-cyanocoumarin and 4-acetylbenzonitrile, where the distances between the CN and CO groups are ≈3.1 and ≈6.5 Å, respectively. A 6-fold increase in cross-peak amplitude was observed in 4-acetylbenzonitrile when the dual-frequency RA 2DIR method was used.

dual-frequency 2D IR | heat transport | vibrational relaxation

Development of new methods for determining the 3D structures of molecules in solution is an important challenge in chemistry. Recently introduced in the pioneering works of Hochstrasser and colleagues (1, 2), two-dimensional infrared (2D IR) spectroscopy has demonstrated its strong potential for measuring molecular structures in solution under physiological conditions (2–10). 2D IR and 2D NMR correlation methods have many analogies (11). The cross-peaks in 2D IR spectra originate from pairwise interactions of vibrational modes (vs. nuclear spins for 2D NMR), offering a measure of the distances between interacting vibrational modes (vs. spins). Readily measurable anisotropy of the cross-peaks in 2D IR reveals another important type of structural information, the mutual orientation of the transition dipoles of interacting modes, *vide infra* (12). Although 2D IR methods have been successfully applied to the study of small molecules and peptides, the measurement of structural constraints in macromolecules such as proteins remains a challenge. Here, we propose a method that uses vibrational relaxation and vibrational energy transport in molecules to significantly enhance the cross-peaks measured with 2D IR for modes separated by distances >4–5 Å. This approach substantially increases the range of distances accessible by 2D IR and is capable of identifying vibrational modes separated by multiple bonds and of delivering the long-range bond connectivity patterns in a way similar to that of the total correlation spectroscopy method of 2D NMR (13) and its heteronuclear version, heteronuclear multiple bond correlation. Relaxation-assisted 2D IR (RA 2DIR) enhances the potential of weak modes in 2D IR and allows their convenient use as structural reporters.

In general, as structural labels, vibrational modes have the advantage of being very compact compared with, for example, FRET labels. However, the choice of vibrational labels for structural measurement in macromolecules by using 2D IR is not obvious. Thus far, most 2D IR cross-peak measurements have been performed by using strong IR stretching modes, such as C≡O, O—H, N—H, and C—N. However, these modes are highly abundant in biopolymers, and isotope substitution is required in order to decouple the label from the rest of the modes. $^{13}C^{18}O$ isotopic substitution in the CO group shifts the CO stretching frequency at ≈1,650 cm^{-1} down by ≈60–65 cm^{-1}, making it a promising vibrational label (14). However, the presence of very strong diagonal CO peaks reduces the dynamic range for the cross-peak measurements, diminishing the range of accessible intermode distances. O—H and N—H modes are less convenient as 2D IR labels because the isotope substitution of nitrogen or oxygen atoms

generates only very small frequency shifts, whereas the protons in these groups are generally exchangeable (10). Labeling with groups not often present in organic molecules, such as N$_3$, has not yet been sufficiently explored in 2D IR. Therefore, although there has been steady progress in 2D IR, including new experimental approaches (15–17),[‡] accessing structural constraints for molecules as large as proteins is still a challenge.

The use of weaker modes as 2D IR labels is promising, although it too is associated with experimental challenges. First, there is a much wider choice of weak modes and labels suitable for particular experimental conditions, including those in the water transparency regions. Second, by selecting mode pairs comprising modes of substantially different frequencies, the cross-peaks can be well separated from the strong diagonal peaks. Diagonal peaks can be largely reduced, or even completely eliminated, by using the dual-frequency 2D IR approach (8, 18). We have recently demonstrated the implementation of weak but localized C≡N stretching modes as structural labels in 2D IR (18). The cross-peaks originating from interactions of CN modes with C≡O and C≡C modes provided convenient structural handles (18).[§] Furthermore, we have shown that extremely weak C—D modes in alkyl groups, having extinction coefficients of only ≈1 M^{-1}·cm^{-1}, form a useful structural reporter, and that interactions among CD and CN modes can be readily measured with dual-frequency 2D IR.[§]

The difficulty in working with weak modes is associated with small cross-peaks, because the cross-peak amplitude is proportional to the square of the weak-mode transition moment. Although the cross-peak amplitude is typically strong enough when the modes are spatially close (18),[§] it is expected to decay rapidly as a function of the mode separation distance (12). A small range of intermode distances accessible by 2D IR using weak IR modes can diminish the applicability of such structural labels. In this article, we describe an approach for measuring 2D IR spectra that allows one to substantially increase the range of distances accessible by 2D IR. The method utilizes vibrational relaxation and intramolecular vibrational energy redistribution (IVR) processes to enhance the cross-peak amplitudes in 2D IR spectra.

Because IVR is the core process that determines the enhancement of the cross-peaks in RA 2DIR, we discuss it briefly here. Vibrational relaxation, energy transfer between specific modes (6,
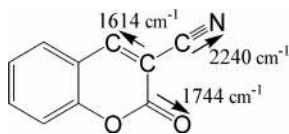
Fig. 1. Structure of 3-cyanocoumarin. The transition moment directions of the modes involved in this study are shown by arrows.

7, 19, 20), and IVR dynamics (19, 21)[¶] in molecules in the condensed phase were studied experimentally and theoretically; recent reviews can be found in refs. 22 and 23. Elegant experiments using Raman detection to follow vibrational energy flow in molecules were performed by Dlott and colleagues (24, 25) The IVR process of high-frequency modes in molecules with more than five atoms, in the condensed phase, was found to be very fast, leading to lifetimes of excited vibrations on the order of 0.5–5 ps (12, 19, 20, 26). The relaxation rates are determined by several factors, including the local density of states, the amplitude and rate of frequency fluctuations, and the intermode coupling matrix elements (22, 23, 26). The complexity of IVR and vibrational energy transport processes originates from the nature of vibrational modes, which are often delocalized in molecules but to a different extent (22, 23, 27). This mode delocalization facilitates mode overlap and increases the rate of the IVR process. On the other hand, the mostly localized character of some modes is a source of fractal effects in proteins that leads to heat confinement effects and anomalous energy transport dynamics (22). Therefore, IVR and energy transport in molecules on the length scales from angstroms to tens of angstroms is complex and less well understood than heat transport on larger scales (28). Although the main advantage of using the RA 2DIR approach lies in its capacity as a structural method, it also provides a convenient means for studying energy transport processes in molecules on angstrom scales. An RA 2DIR method is proposed here and is tested on CN and CO mode interactions in 3-cyanocoumarin and 4-acetylbenzonitrile (AcPhCN).

Results and Discussion

The linear IR spectrum of 3-cyanocoumarin (Fig. 1) is shown in Fig. 2. Three vibrational modes are of importance for this work: C≡N (2,240 cm^{-1}), C=O (1,744 cm^{-1}), and C=C (1,613.7 cm^{-1}); the latter bond is located at the third and fourth coumarin-ring carbon atoms (Fig. 1). For both samples, 3-cyanocoumarin and AcPhCN, the optical density at the CO peaks was 0.3–0.4. For the cross-peak measurements, the pulse spectra were tuned so that the k_1 and k_2 beams overlapped with the CN peak and the k_3 and local oscillator (LO) beams overlapped with the CO peak (Fig. 2).

Qualitative Analysis of the 2D IR Spectrum at T = 670 fs. The dual-frequency absorptive spectrum of 3-cyanocoumarin obtained at time delay T (T-delay) of 670 fs is shown in Fig. 3A. The spectra of the mid-IR pulses used for this experiment are shown in Fig. 2. Three pairs of peaks are prominent. The pair at approximately (1,743, 2,239), originating from the interaction of the CN and CO modes, dominates the spectrum. Surprisingly, the diagonal CO-mode peaks can also be seen at approximately (1,743, 1,743 cm^{-1}). The diagonal peaks are observed because the k_1, k_2 pulses, centered at 2,239 cm^{-1}, have nonzero intensity at 1,743 cm^{-1} that only amounts to 2×10^{-3} of the intensity of 2,239 cm^{-1} maximum. The amplitude of the diagonal peaks increases $\approx$500 times when the k_1, k_2 spectra are centered at 1,743 cm^{-1}.

In addition, another cross-peak pair, which is derived from interaction of the CN and CC modes, is seen in the 2D spectrum at approximately (1,605, 2,239 cm^{-1}) (Fig. 3A). The amplitude of

[¶]Kim, Y. S., Hochstrasser, R. M., 15th International Conference on Ultrafast Phenomena, Optical Society of America, July 31–Aug. 4, 2006, Pacific Grove, CA.
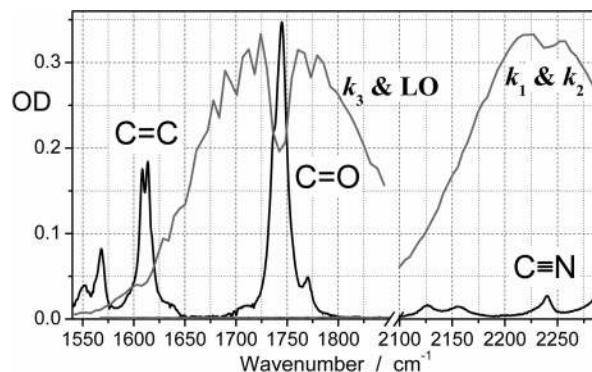
Fig. 2. Linear spectrum of 3-cyanocoumarin and the spectra of the IR pulses tuned to match the CN and CO bands.

this peak is only $\approx$2 times smaller than that of the CO/CN cross-peaks, whereas the intensity of the k_3 and LO pulses at ω_{CC} is >5 times smaller than that at ω_{CO}, indicating that interaction among the CC and CN modes is substantially stronger than interaction among the CO and CN modes.

Several characteristics of the 2D IR spectra can be used to determine the off-diagonal anharmonicity values. One is the amplitude of the cross-peaks relative to the amplitude of the diagonal peaks. By using the measured light intensities of all pulses at the wavelengths involved, as well as the known value of diagonal anharmonicity of the CO mode, the CN/CO off-diagonal anharmonicity can be obtained by global modeling.

Alternatively, the exact frequencies of the peaks in 2D IR spectra can provide an estimate of the off-diagonal anharmonicities. Note that the peak separation in a peak pair reveals the respective anharmonicity only if the anharmonicity is larger then the width of the transition at ω_t. When the off-diagonal anharmonicity is small compared with the linewidths, the peak separation in the peak pair is determined solely by the width of the transition (19). However, the relative positions (ω_t) of the diagonal and cross-peaks can be used to determine the anharmonicities. Specifically, the ω_t frequency of the crossing-point on the zero contour and the line connecting the minimum and maximum in the peak pair, denoted as ω_t^z, is very informative (Fig. 3). The diagonal CO peaks are formed by the negative peak at (ω_{CO}, ω_{CO}) and the positive peak at ($\omega_{CO} - \Delta_{CO}$, ω_{CO}), where ω_{CO} and Δ_{CO} are the 0→1 transition frequency and the diagonal anharmonicity of the CO mode, respectively (Fig. 4 B and C). If the difference in width and amplitude for the positive and negative peaks of a peak pair are neglected (weak anharmonicity limit), the ω_t^z frequency is located in the middle, between the two peaks. Therefore, for the diagonal CO peak, the ω_t^z frequency equals $\omega_{CO} - \frac{1}{2}\Delta_{CO}$. The CO/CN cross-peaks are also formed by two peaks: the negative peak at (ω_{CO}, ω_{CN}) and the positive peak at ($\omega_{CO} - \Delta_{CN/CO}$, ω_{CN}), where ω_{CN} is the 0→1 transition frequency of the CN mode and $\Delta_{CN/CO}$ is the off-diagonal anharmonicity for the CN/CO interaction. The ω_t^z frequency of the CN/CO cross-peak is also in the middle, between the ω_{CO} and $\omega_{CO} - \Delta_{CN/CO}$ frequencies, namely at $\omega_{CO} - \frac{1}{2}\Delta_{CN/CO}$. Therefore, the shift between the ω_t^z frequencies for the diagonal and the cross-peaks is expected to be [ω_t^z(cross) − ω_t^z(CO) = $\frac{1}{2}(\Delta_{CO} - \Delta_{CN/CO})$]. The experimental value of the shift of 6.5 ± 0.5 cm^{-1} measured in the T = 670 fs spectrum (Fig. 3A) provides an estimate of the off-diagonal anharmonicity at 2 ± 1 cm^{-1}.

Two-Dimensional IR Spectra Measured at Various T-Delay Times: Qualitative Analysis. To investigate how vibrational relaxation dynamics affect the spectra, we measured the 2D IR spectra at several T-delays, two of which, T = 2 and 4 ps, are shown in Fig. 3. As
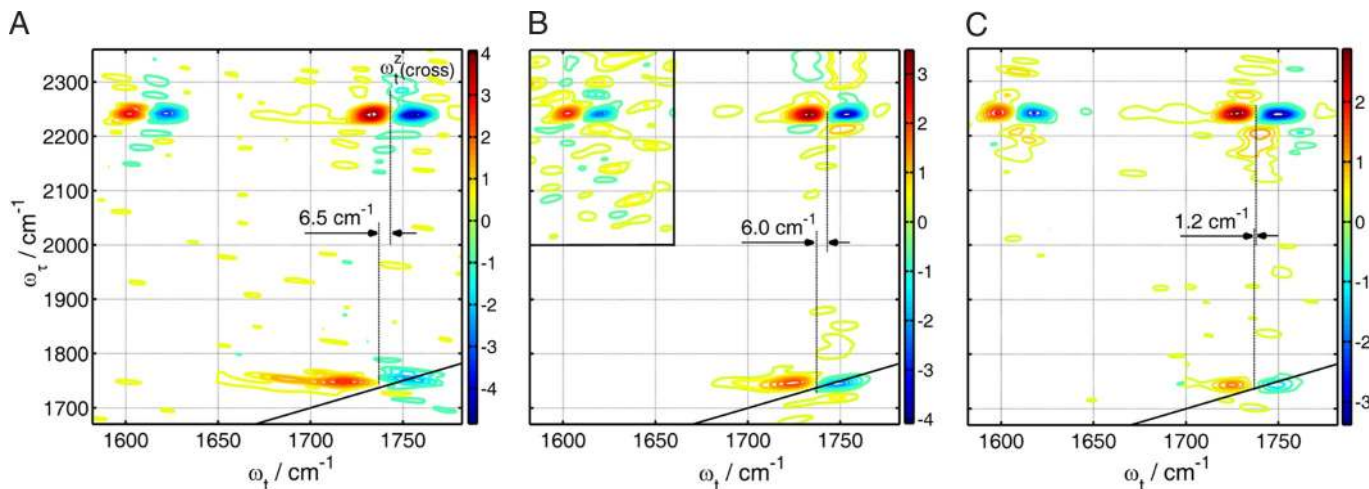
Fig. 3. Two-dimensional IR absorptive spectra of cyanocoumarin measured at T-delays of 670 fs (*A*), 2 ps (*B*), and 4 ps (*C*). The zero-contour ω_t^z frequencies are shown. In *B Inset*, the amplitude of the upper-left part of the spectrum was multiplied by a factor of 3.

expected, these spectra exhibit peaks similar to those seen in the spectrum obtained at $T = 670$ fs, but surprisingly the amplitudes of these peaks are almost as large as those in the $T = 670$ fs spectrum. Indeed, the lifetime of the excited CN mode has been measured at 1.4 ± 0.2 ps by a pump-probe method. The CN excited-state population at a T-delay of 4 ps drops by $\approx$20-fold, and the cross-peak amplitude in the $T = 4$ ps spectrum is expected to be >10 times smaller than that in the $T = 670$ fs spectrum. Because such decrease was not observed experimentally, we concluded that vibrational relaxation and IVR processes, which have little influence on the spectra with small T values, are strongly affecting those measured at large T-delays.

In addition to weakly decreasing the CO/CN cross-peak amplitude in the spectra at 0.67, 2, and 4 ps T-delay, the ω_t^z frequency of the CO/CN cross-peak changes with the T-delay. The following qualitative analysis of the spectra at various T-delays is based on comparison of the ω_t^z frequencies for the CO-diagonal [ω_t^z(CO)] and CN/CO-cross [ω_t^z(cross)] peaks. The shift value [ω_t^z(cross) $-$ ω_t^z(CO)] changes from 6.5 ± 1 cm^{-1} in the $T = 670$ fs spectrum to 6 ± 1 cm^{-1} and 1.2 ± 0.5 cm^{-1} in the spectra at 2 and 4 ps, respectively. At $T = 4$ ps, the major part of the excited CN mode population has been relaxed by the IVR process to other modes, mainly those in the same molecule. Vibrational relaxation can populate the modes, denoted as X, that are strongly coupled to the

CO mode and that therefore have large CO/X anharmonicities, $\Delta_{X/CO}$ (Fig. 4*A*). We concluded that the cross-peaks at large T-delays derive from interactions of such modes, X, with the CO mode. Typical Feynman diagrams responsible for such cross-peaks are shown in Fig. 4 *C* and *D*. The experimentally observed drastic shift of ω_t^z to smaller frequencies indicates that IVR populates the modes, X, that have $\Delta_{X/CO}$ anharmonicities larger than the direct-coupling CN/CO anharmonicity, $\Delta_{CO/CN}$. Note that the amplitude of the cross-peaks remains nearly unchanged until $T \approx 6$ ps, whereas the peak character changes from the direct-coupling (Fig. 4 *B* and *C*) to the relaxation-induced cross-peaks (Fig. 4 *C* and *D*).

Vibrational relaxation from the CN mode can also lead to population of the CO mode (X≡CO); however, modeling showed that such a relaxation pathway is not the dominant pathway. The X state comprises a variety of yet-unidentified modes interacting with the CO mode, and the off-diagonal anharmonicity $\Delta_{X/CO}$ represents an averaged anharmonicity over multiple states populated by IVR. However, because the amplitude of the cross-peaks featuring small anharmonicities is proportional to the anharmonicity value, strong interactions with large anharmonicities dominate the cross-peak.

To clarify various contributions to the cross-peaks at longer T-delays, the rephasing (ω_t, T) 2D spectra were measured. The ω_t spectra acquired in this way include contributions from all peaks with the same ω_t that appeared in the 2D spectrum measured under the same experimental conditions. In other words, the ω_t spectrum is a sort of projection of the 2D spectrum onto the ω_t axis. Therefore, the CO peak in the ω_t spectra, although dominated by CN/CO cross-peaks, also contains contributions from the CO-diagonal peaks. A shift to smaller frequencies at larger T values was observed for both the CO and CC peaks [see supporting information (SI) Fig. 10]. The peak amplitude and peak frequency are plotted for both peaks as a function of T-delay (Fig. 5). An interference of the cross-peak and diagonal-peak contributions, seen as an oscillatory pattern, was introduced by small changes in τ values for the scans at different T-delays.

Interestingly, the two dependencies (i.e., the peak amplitude and the peak frequency) have very different time behaviors. The amplitudes of both the CO and CC peaks decay with the characteristic time of $\approx$14 ps, which is much longer than the CN excited-state lifetime ($T_1^{CN} = 1.4$ ps). The peak frequencies of both peaks shift to smaller values by $\approx$3–4 ps. The shift is $\approx$7 cm^{-1} for the CO peak and $\approx$4 cm^{-1} for the CC peak. Note that the peak frequency of the absolute-value spectrum is approximately equal to the ω_t^z frequency of the peak pairs. The shift occurs when the relaxation-induced peaks overcome the direct-coupling cross-
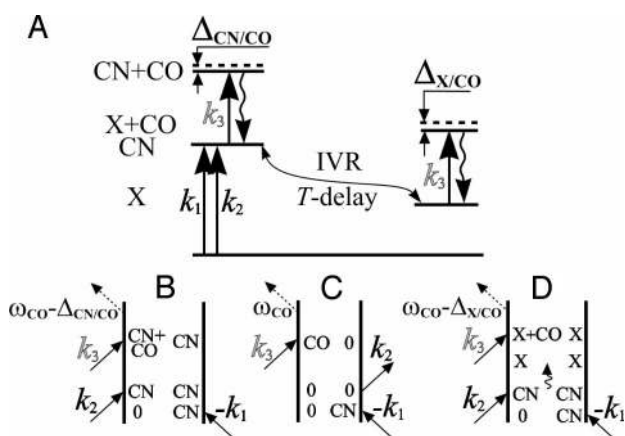

Fig. 4. Energy diagram (*A*) and rephasing Liouville pathways describing the direct-coupling (*B* and *C*) and relaxation-assisted (*C* and *D*) cross-peaks.
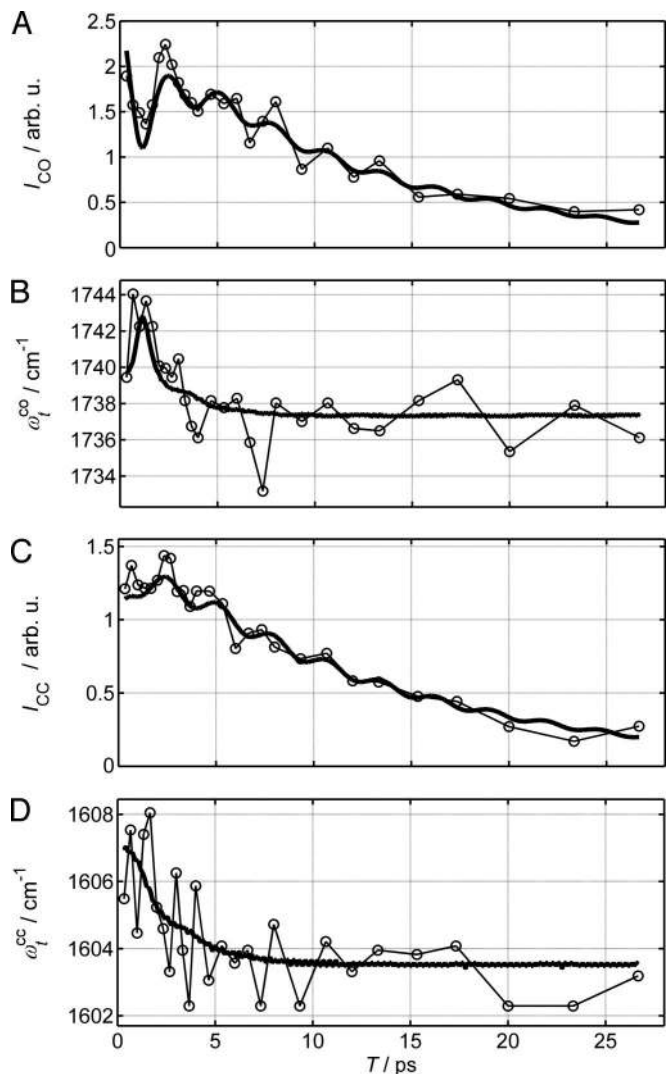
Fig. 5. CO (*A*) and CC (*C*) peak amplitudes and CO (*B*) and CC (*D*) peak frequencies as a function of T-delay, obtained from the dual-frequency (ω_t, *T*) spectrum. The heavy line represents the results of global modeling with the following parameters: $k_{CN/CO} = (30\text{ ps})^{-1}$, $k_{CN/CC} = (4.3\text{ ps})^{-1}$, $k_{CN/X} = (7.9\text{ ps})^{-1}$, $k_{CN/gr} = (3.7\text{ ps})^{-1}$, $k_{CO/CC} = (2.5\text{ ps})^{-1}$, $k_{CO/X} = (3.6\text{ ps})^{-1}$, $k_{CO/gr} = (4.8\text{ ps})^{-1}$, $k_{CC/X} = (7.6\text{ ps})^{-1}$, $k_{CC/gr} = (8.2\text{ ps})^{-1}$, $k_{X/gr} = (27.6\text{ ps})^{-1}$, $\Delta_{CO/CN} = 2 \pm 0.5\text{ cm}^{-1}$, $\Delta_{CN/CC} = 12 \pm 3\text{ cm}^{-1}$, $\Delta_{CO/CC} = 0.9 \pm 0.2\text{ cm}^{-1}$, $\Delta_{X/CO} = 0.4 \pm 0.1\text{ cm}^{-1}$, $\Delta_{CC/X} = 18 \pm 0.2\text{ cm}^{-1}$, $\Delta_{CO} = 14 \pm 1.5\text{ cm}^{-1}$, $\Delta_{CC} = 17 \pm 2\text{ cm}^{-1}$, and $E_X = 1,420\text{ cm}^{-1}$.

peaks. Therefore, at T-delays >3–4 ps, the contributions from the excited states populated by IVR dominate the cross-peaks; even at 5 ps, the amplitude of the cross-peaks is very strong.

Spectral Modeling and Relaxation Scheme

The heterodyned time-domain third-order signal giving rise to cross-peaks at (ω_1, ω_2) in the Bloch approximation is given by

$$S_{R/NR}(\tau, T, t) = \langle zzzz\rangle \mu_1^2 \mu_2^2 e^{i(\pm\omega_1\tau - \omega_2 t)}$$
$$\cdot [e^{i\Delta_{12}t}e^{-t/T_1^{(1)}} - 1]e^{-\gamma_1\tau - \gamma_2 t - \sigma_1^2\tau^2/2 - \sigma_2^2 t^2/2 - T/T_1^{(1)}}e^{\pm f\sigma_1\sigma_2 t\tau}, \quad [1]$$

where the upper and lower signs correspond to the rephasing and nonrephasing experiments, respectively; $\langle zzzz\rangle = 1 + \frac{2}{5}(3\cos^2\theta - 1)e^{-T/\langle\tau\rangle}$ is the rotation relaxation factor for *z* polarization for all four pulses (29); $\langle\tau\rangle$ is the mean rotation time; Δ_{12} is the off-diagonal anharmonicity; $T_1^{(1)}$ is the population relaxation time of the ω_1 mode; and $\gamma_{1,2}$, $\sigma_{1,2}$, and $\mu_{1,2}$ are the
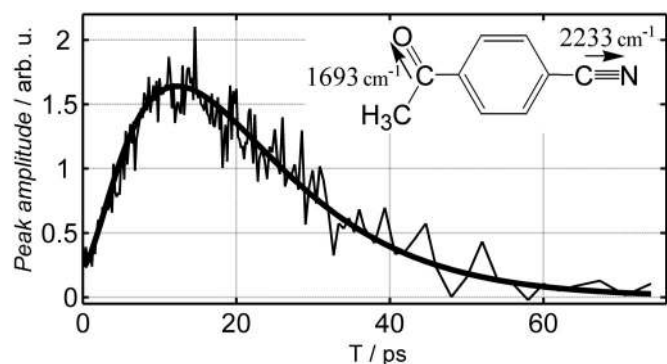
Fig. 6. CO peak amplitude for AcPhCN as a function of T-delay, obtained from the (ω_t, *T*) dual-frequency spectra.

total dephasing time, inhomogeneous width, and transition dipole of the fundamental transitions with ω_1 and ω_2 frequencies, respectively. The distributions of ω_1 and ω_2 frequencies were assumed to be static, with the correlation coefficient *f* given by $\langle\delta\omega_1\delta\omega_2\rangle/\sigma_1\sigma_2$, where $\delta\omega_{1,2}$ are the frequency deviations from the respective mean frequencies. The diagonal signals were also modeled with Eq. **1**, taking $\mu_2 = \sqrt{2}\mu_1, f = 1$ (9, 30), $\omega_2 = \omega_1$, and $\Delta_{12} = \Delta_{11}$, where Δ_{11} is the value of the diagonal anharmonicity. Note that the CN/CO cross-peaks measured with *zzzz* polarizations are not very sensitive to rotational motion in both 3-cyanocoumarin and AcPhCN. This is because the angle between the transition moments of the CN and CO modes in both compounds is ≈60°, which is close to the magic angle. Therefore, the amplitude of the cross-peak is expected to change, as a result of rotational relaxation, by only ≈10%. Also, orientational motion during τ and *t* time intervals does not significantly influence the signals because the mean rotation time in methylene chloride was estimated to be >6 ps for both compounds (31), which is much larger than the τ and *t* scanning ranges.

A minimal relaxation scheme sufficient to describe all spectral features includes four modes: CN, CO, CC, and X. For every pair of modes, A and B, the rate constant of the A-to-B reaction (k_{AB}) was connected with the B-to-A reaction rate constant (k_{BA}) through the Boltzmann factor, $k_{AB}/k_{BA} = \exp[\hbar(\omega_A - \omega_B)/kT]$. The pairwise interactions among the four modes were explicitly included. The values of the lifetimes for the CN, CO, and CC modes were allowed to change within the error bars to their experimentally measured values of 1.4, 1.3, and 2.2 ps, respectively. Six experimental dependencies (i.e., the four shown in Fig. 5 plus the linear spectrum and the CN population delay) were fitted globally. The parameters obtained (see Fig. 5 legend) were used to generate the fitting curves (Fig. 5). The fit required having a state that remains excited for >25 ps and is strongly coupled to the CO mode. The lifetime of the X state (≈27 ps) can be understood as the cooling time of the molecule. The cooling time is known to depend on the amount of vibrational excess energy and may aid in the identification of energy range for the X mode (20).

CN/CO Cross-Peaks for AcPhCN.
Dual-frequency 2D IR measurements were performed on the CN and CO modes in AcPhCN. As expected, the direct-coupling CN/CO cross-peaks for modes separated by ≈6.5 Å appeared to be very weak and noisy. However, with an increase in the T-delay, *T*, the cross-peak amplitude increases >6-fold because of the appearance of the relaxation-assisted cross-peaks (Fig. 6). Large enhancement for relaxation-assisted cross-peaks is observed as a result of the large distance between the modes; the direct coupling at such distances is small, but vibrational excitation transferred from the excited CN modes can reach the CO site efficiently. The cross-peak amplitude reaches
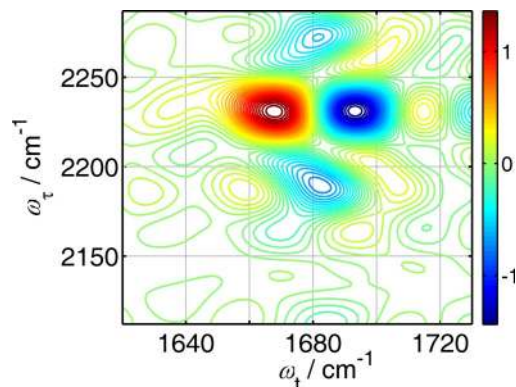
Kurochkin *et al.*

Fig. 7. RA 2DIR absorptive spectrum of AcPhCN, measured at T = 11 ps.

a maximum at ≈12 ps: the time needed to excite the modes that are strongly coupled to the CO mode. The cross-peak of AcPhCN measured at T = 11 ps (Fig. 7) has only a 3-fold smaller amplitude than the direct-coupling cross-peak in cyanocoumarin measured at T = 300 fs, although the CN–CO intermode distance is >2 times larger. The solid line in Fig. 6 represents the modeling results, in which the induction time observed in the cross-peak amplitude growth was reproduced by incorporating one additions mode, X^*, and the dominating sequential relaxation pathway, $CN \rightleftharpoons X \rightleftharpoons X^*$. Because the energy transport model used is oversimplified, the parameters obtained are not shown. A comparison of the cross-peak amplitudes for the two samples allowed us to determine, by modeling, that the direct-coupling anharmonicity $\Delta_{CO/CN}$ in AcPhCN is 0.03 ± 0.01 cm^{-1}.

The cross-peak amplitude T-delay dynamics (Fig. 6) show that vibrational excitation is preserved in the molecule for >40 ps. Because the typical lifetime of high-frequency modes in large organic molecules is ≈0.5–2 ps, a large number of IVR exchange steps must occur during a 10-ps time window. These relaxation steps are responsible for propagation of the excess energy along the molecule. It is known that vibrational energy equilibration and transport dominantly proceed along covalent bonds in a molecule (20, 22, 28). Energy transfer to the solvent is about an order of magnitude slower because the mechanical through-bond coupling of spatially overlapping modes in a molecule is typically much stronger than the through-space electric coupling with solvent modes. In other words, molecules behave as good heat conductors reasonably well isolated from the solvent. The relaxation pathways across the molecule from the initially excited localized ω_1 mode are shown schematically in Fig. 8. The delocalization and spatial overlap of the modes involved in IVR are important factors for vibrational energy propagation. After a small number of IVR steps, the modes
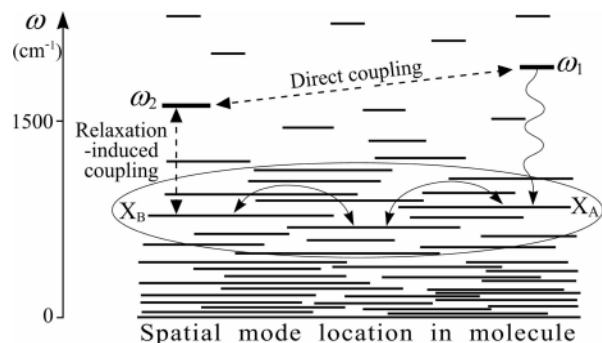

Fig. 8. Schematic representation of fundamental vibrational states as a function of their location in a molecule. Horizontal bars show spatial extent of vibrational modes.

residing on the same atoms as the ω_2 mode get excited. Even if the frequencies of these modes are much smaller than the frequency of the CO mode, the mechanical coupling with CO is expected to be strong because the modes reside on the same atoms. We suggest that excitation of such modes gives rise to the RA 2DIR cross-peaks. Specifically, for AcPhCN, the in-plane and out-of-plane CO bending and rocking modes of the acetyl group seem to be the most probable candidates for the cross-peak contributions. Note that the excitation energy of a high-frequency mode such as CN is sufficient to excite two to five medium-frequency vibrations, which increases relaxation-assisted cross-peak amplitudes.

Structural Constraints Accessible with RA 2DIR. The RA 2DIR method relies on vibrational relaxation and IVR processes for generating stronger cross-peaks. The cross-peaks measured by RA 2DIR appear at the frequencies of the modes excited by IR pulses. However, the (ω_2, ω_1) cross-peak amplitude does not reveal the interaction of the ω_1 and ω_2 modes but instead reflects interactions of the ω_2 mode (CO in this work) with the modes that are populated by IVR processes from the initially excited ω_1 mode (CN in this work). Nevertheless, structural constraints other than the coupling can be measured with RA 2DIR. The cross-peak anisotropy provides a measure of the angle between the transition dipoles of the modes accessed with IR pulses (CN and CO in this work) in exactly the same way as for the direct-coupling cross-peaks. The first two pulses, linearly polarized along the same axis, act on the ω_1 mode and prepare the anisotropically excited sample in the laboratory frame, an effect known as "photoselection." If the transition dipole of the ω_2 mode has specific orientation in the molecule with respect to that of the ω_1 mode, the ω_2 modes of the excited molecules will be anisotropically distributed in the laboratory frame as well. This anisotropy can be measured by polarized pulses probing the ω_2 mode, and the mean angle between the ω_1 and ω_2 transition dipoles can be recovered (12). One can measure the anisotropic angular distribution on the ω_2 mode created in the excited molecules by photoselection on the ω_1 mode only if the ω_2 frequency is somewhat affected by the ω_1 excitation; otherwise, the photoselected and nonselected molecules cannot be separated. The direct ω_1-to-ω_2 coupling, or the indirect influence on the ω_2 frequency through excitation of a mode (ω_X) that is coupled to the ω_2 mode, could be responsible for this phenomena. Either way, the anisotropy measurements are only sensitive to the mutual orientation of modes ω_1 and ω_2, accessed by light, regardless of the origin of the influence. Therefore, the anisotropy of the (ω_2, ω_1) cross-peak in RA 2DIR spectra is indicative of the angle between transition moments for the ω_1 and ω_2 modes. Rotational motion during the waiting time, T, will cause anisotropy decay, smearing-out the angular information. This is not a problem in proteins, in which rotational motion is typically much slower (32). Viscous solvents and/or lower temperatures could be used to determine the angles in small molecules by using RA 2DIR.

The T-delay value at which the cross-peak amplitude reaches its maximum (arrival time) reveals the bond connectivity and can be correlated with the distance between the modes. Different scenarios can occur, depending on the type of vibrational modes present in the molecule and their coupling and frequency range (28). One could imagine highly resonant cases in which energy propagates very fast, hopping between resonant delocalized modes. Although in such a regime it might be difficult to correlate the arrival time with the distance, the vibrational energy can migrate greater distances without substantial dissipation, which may enhance the range of distances accessible in RA 2DIR studies. In another limiting case, the energy flow might be almost diffusional, with the excess energy being treated as heat, as is expected at larger distances from the excitation source and at smaller excess energies (28). Intermediate cases are likely to occur (22, 25, 28), and theoretical modeling is required in order to correlate the energy arrival time with the distance between the groups.
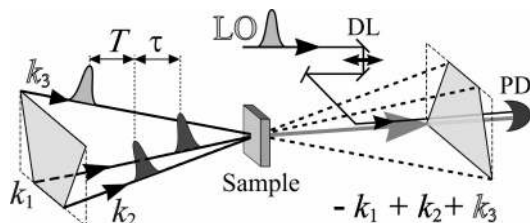
Fig. 9. Pulse geometry for the dual-frequency 2D IR experiments with the k_1 and k_2 pulses centered at 4 μm and the k_3 and LO pulses centered at 6 μm.

It is interesting to speculate how strong enhancement of the cross-peak amplitude can be achieved. Clearly it depends on the type of modes used, the initial distance between the modes, and the size and structure of the molecule. In the limiting case that the energy transport along the molecule can be described as heat diffusion, a simple estimation can be performed. For linear molecules in which heat transport can be treated as pseudo-1D, the maximal temperature reached at distance R from the initial heating spot depends on distance as R^{-1}. Although such a weak distance-dependence is encouraging, the actual RA 2DIR cross-peak amplitude depends on the frequencies of the modes (ω_X) coupled with the ω_2 mode (CO in this work). On the other hand, the distance-dependence for the direct-coupling peaks depends on the coupling mechanism. For the electric coupling of the modes that are far from resonance, the off-diagonal anharmonicity depends on the distance between the interacting modes as R^{-6} (12). Mechanical coupling distance-dependence is not well understood. Interestingly, the values of the off-diagonal anharmonicity measured for cyanocoumarin and AcPhCN are in agreement with the $R^{-5.7}$ distance-dependence, even though mechanical coupling is the dominant coupling mechanism. Estimations show that >20-fold enhancements of the cross-peak amplitudes might be possible using the RA 2DIR approach.

Conclusions

Interestingly, the cross-peaks caused by vibrational relaxation in 2D IR spectra have been observed before (6, 7, 19, 20),¶ but their capabilities for structural measurement have not been foreseen. We analyzed the relaxation phenomena and found that, under certain experimental design conditions, it can lead to a very strong enhancement of cross-peak amplitudes. Here we have proposed an RA 2DIR structural method and have demonstrated that it can provide a useful handle in measuring weak mode-to-mode interactions in molecules and can deliver cross-peaks that are much

stronger than direct-coupling cross-peaks. This enhancement will allow observation of cross-peaks for modes separated by large distances. It is conceivable that >3 times larger distances will be accessible with RA 2DIR than with traditional 2D IR. Two types of structural constraints can be measured by using RA 2DIR cross-peaks. First, the angles between transition moments of the modes accessed by IR pulses can be determined by anisotropy measurements, in the same way as for the direct-coupling peaks. Second, the T-delay dependence of the cross-peak amplitude (Fig. 6) could be related to the distance between the groups by using theoretical modeling. We also suggest that the most probable candidates for the modes accepting vibrational energy and strongly coupled to the CO mode are those located on the same atoms as CO, specifically, the acetyl in-plane and out-of-plane bending and rocking modes. The RA 2DIR method can be implemented in various experimental settings, including the 2D IR pump-probe setup.

Experimental Methods

Dual-Frequency Heterodyned 2D IR Spectra. The geometry of pulses used for the dual-frequency 2D IR experiments, and the notations used for the delays between the pulses, are shown in Fig. 9. The technical details of the pulse generation are given in *SI Experimental Methods*. The third-order signal emitted by the sample was picked at the phase-matching direction ($-k_1 + k_2 + k_3$) and mixed on a detector with the LO. The 2D (t, τ) spectra were recorded and double Fourier-transformed to obtain (ω_t, ω_τ) spectra. The rephasing spectra were collected, with the k_1 pulse arriving first and the k_2 pulse arriving second; for the nonrephasing spectra, the order of the first two pulses was reversed. The polarization direction was the same for all four beams. Absorptive 2D spectra were constructed as a sum of the real parts of the rephasing and nonrephasing spectra.

The (ω_t, T) spectra were obtained by a Fourier transformation of the (t, T) 2D array along the t direction. The τ delay in the measurements of the (t, T) array was varied in relation to the T-delay, according to the equation, $\tau = 10 + 0.024 \times T$ fs. The modeling of these spectra was performed by using the same conditions.

Sample Preparation. The samples were 89 mM 3-cyanocoumarin and 125 mM AcPhCN in dichloromethane, held in a 50-μm optical path length cell with CaF$_2$ windows.

1. Hamm P, Lim M, Hochstrasser RM (1998) *J Phys Chem B* 102:6123–6138.
2. Asplund MC, Zanni MT, Hochstrasser RM (2000) *Proc Natl Acad Sci USA* 97:8219–8224.
3. Mukamel S (1995) *Principles of Nonlinear Spectroscopy* (Oxford Univ Press, New York).
4. Golonzka O, Khalil M, Demirdoven N, Tokmakoff A (2001) *J Chem Phys* 115:10814–10828.
5. Gaffney KJ, Piletic IR, Fayer MD (2002) *J Phys Chem A* 106:9428–9435.
6. Khalil M, Demirdoven N, Tokmakoff A (2004) *J Chem Phys* 121:362–373.
7. Schanz R, Botan V, Hamm P (2005) *J Chem Phys* 122:044509/1–044509/10.
8. Rubtsov IV, Wang J, Hochstrasser RM (2003) *Proc Natl Acad Sci USA* 100:5601–5606.
9. Rubtsov IV, Wang J, Hochstrasser RM (2003) *J Phys Chem A* 107:3384–3396.
10. Asbury JB, Steinel T, Fayer MD (2004) *J Phys Chem B* 108:6544–6554.
11. Scheurer C, Mukamel S (2002) *J Chem Phys* 116:6803–6816.
12. Hamm P, Hochstrasser RM (2000) in *Ultrafast Infrared and Raman Spectroscopy*, ed Fayer MD (Marcel Dekker, New York), pp 273–347.
13. Ernst RR, Bodenhausen G, Wokaun A (1987) *Principles of Nuclear Magnetic Resonance in One and Two Dimensions* (Oxford Univ Press, New York).
14. Paul C, Wang J, Wimley WC, Hochstrasser RM, Axelsen PH (2004) *J Am Chem Soc* 126:5843–5850.
15. Fulmer EC, Ding F, Zanni MT (2005) *J Chem Phys* 122:034302/1–034302/12.
16. Bredenbeck J, Helbing J, Sieg A, Schrader T, Zinth W, Renner C, Behrendt R, Moroder L, Wachtveit J, Hamm P (2003) *Proc Natl Acad Sci USA* 100:6452–6457.
17. Hamm P (2006) *J Chem Phys* 124:124506/1–124506/13.
18. Kurochkin DV, Naraharisetty SG, Rubtsov IV (2005) *J Phys Chem A* 109:10799–10802.
19. Rubtsov IV, Hochstrasser RM (2002) *J Phys Chem B* 106:9165–9171.
20. Nibbering ETJ, Elsaesser T (2004) *Chem Rev* 104:1887–1914.
21. Brixner T, Stenger J, Vaswani HM, Cho M, Blankenship RE, Fleming GR (2005) *Nature* 434:625–628.
22. Leitner DM (2005) *Adv Chem Phys* 130:B205–B256.
23. Fujisaki H, Straub JE (2005) *Proc Natl Acad Sci USA* 102:6726–6731.
24. Wang Z, Pakoulev A, Dlott DD (2002) *Science* 296:2201–2203.
25. Deak JC, Pang Y, Sechler TD, Wang Z, Dlott DD (2004) *Science* 306:473–476.
26. Fujisaki H, Zhang Y, Straub JE (2006) *J Chem Phys* 124:144910/1–144910/11.
27. Engholm JR, Rella CW, Schwettman HA, Happek U (1996) *Phys Rev Lett* 77:1302–1305.
28. Gruebele M, Wolynes PG (2004) *Acc Chem Res* 37:261–267.
29. Hochstrasser RM (2001) *Chem Phys* 266:273–284.
30. Hamm P, Lim M, Hochstrasser RM (1998) *Phys Rev Lett* 81:5326–5328.
31. Horng M-L, Gardecki JA, Maroncelli M (1997) *J Phys Chem A* 101:1030–1047.
32. Lakowicz JR (1983) *Principles of Fluorescence Spectroscopy* (Plenum, New York).